# Pygmy Dipole Modes in Shape-Coexisting $^{40}$Mg

**Kai Wang and Junchen Pei**

*State Key Laboratory of Nuclear Physics and Technology, School of Physics, Peking University, Beijing 100871, China*

**Abstract**

Weakly bound nuclei have exotic collective excitations associated with halo structures and continuum effects. Our study of isovector dipole modes in the shape-coexisting $^{40}$Mg is based on the fully self-consistent continuum FAM-QRPA in deformed large coordinate spaces. The $K$-splitting in low-lying pygmy resonances clearly deviates from the proportionality in terms of static deformations which is inherent for giant resonances.

**Keywords:** *Collective excitation; FAM-QPRA; shape-coexistence*

## 1 Introduction

Quantum many-body systems have emergent amazing macroscopic phenomena that can not be easily derived from their constituent parts [1]. Nuclei are in an evolution from few-body to many-body systems, and can possess deformed shapes and superfluidity which can enhance essentially the nuclear collective behavior [2]. Thus, an accurate treatment of continuum in large coordinate spaces is essential for the description of collective excitation modes in weakly bound nuclei.

A traditional way to implement the QRPA is the matrix diagonalization scheme (MQRPA). However, huge dimensions of the QRPA matrix, especially when the spherical symmetry is broken and continuum configurations are included, result in expensive computational costs, which become a major numerical challenge.

To this end, the finite amplitude method (FAM), which allows us to compute all induced fields using a finite difference method employing a subroutine of the static mean-field Hamiltonian, is introduced to calculate strength functions [3]. The FAM-QRPA for monopole modes has been implemented based on several well-known DFT-solvers, such as the spherical coordinate-space program HFBRAD, the deformed harmonic oscillator basis space program HFBTHO, and the deformed relativistic Hartree–Bogoliubov method [3, 4]. Previously, we also developed the FAM-QRPA based on our DFT-solver HFB-AX which provides very precise ground-state HFB solutions in the deformed coordinate space [5]. Recently M. Kortelainen *et al.* extended the FAM to a deformed multipole case, allowing the evaluation of QRPA modes for operators of arbitrary multipolarity $LK$ with simplex-$y$ basis [6]. Now we also extend our FAM-QRPA to multipole excitation modes based on the HFB-AX, which provides a good resolution of quasiparticle resonances and continuum spectra due to

*Proceedings of the International Conference 'Nuclear Theory in the Supercomputing Era — 2016' (NTSE-2016), Khabarovsk, Russia, September 19–23, 2016. Eds. A. M. Shirokov and A. I. Mazur. Pacific National University, Khabarovsk, Russia, 2018, p. 174.*

*http://www.ntse-2016.khb.ru/Proc/Pei.pdf.*

large box sizes and dense lattices [7]. This is an ideal tool for describing the collective excitations of weakly bound deformed nuclei.

$^{40}$Mg is the last experimentally observed magnesium isotope [8] with an $N = 28$ magic neutron number, but with a well-established prolate-oblate shape-coexistence [9, 10]. Such a shape-coexistence is ideal for a comparative analysis of deformation-related isovector dipole (IVD) modes, which are a natural probe of surface oscillations and are directly related to the photoabsorption cross section.

## 2 Theoretical models

As mentioned above, the HFB equation is solved by HFB-AX [11] within a large two-dimensional coordinate space based on B-spline techniques with an assumed axial symmetry. The mesh distance is 0.6 fm and the order of B-spline is 12. A hybrid MPI + OpenMP parallel scheme was utilized to get converged results within a reasonable time.

For the particle-hole interaction channel, a recently adjusted extended SLy4 force for light nuclei is adopted [12] including an additional density-dependent term. For the particle-particle channel, a density dependent delta interaction (DDDI) [13], $V_0[1 - \eta(\rho(\mathbf{r})/\rho_0)^\gamma]$, is used. With a pairing window of 60 MeV, the pairing force parameters are taken as $V_0 = -448.3$ MeV fm$^3$, $\eta$=0.8 and $\gamma$=0.7, so that pairing gaps in both stable and very neutron-rich nuclei can be properly described. The resulted pairing gaps are between those from mixed and surface types of pairing in very neutron-rich nuclei, while the surface pairing interaction may overestimate pairing correlations in nuclei far from stability [14].

The next step is to calculate a strength function within the framework of FAM-QRPA utilizing the wave functions obtained by HFB-AX. The same parameters in the particle-hole and particle-particle channels are used in the DFT-solver and FAM for self-consistency. To study the fine structures of pygmy resonances, the smoothing parameter is taken to be 0.25 MeV (cf. with the usually adopted value of 0.5 MeV). For each frequency point $\omega$, the calculation employs the OpenMP shared memory parallel scheme. For different frequencies, the MPI distributed parallel scheme is adopted. All computations are performed on the Tianhe-1A supercomputer located in Tianjin and Tianhe-2 supercomputer located in Guangzhou.

## 3 Results

As is seen from Table 1, the oblate shape is 1.9 MeV above the prolate shape reflecting the fact that $^{40}$Mg has a soft potential energy surface. The shape competition is also reflected in the superfluidity difference: the prolate shape only has a neutron pairing gap while the oblate shape only has a proton pairing gap.

The neutron density and neutron pairing density distributions in $^{40}$Mg in different shape are shown in Fig. 1. The densities are displayed along the cylindrical coordinates $z$ (symmetrical axis) and $r = \sqrt{x^2 + y^2}$ (perpendicular to the symmetrical axis), respectively. The difference between two profiles reflects the surface deformation. The absolute value of pairing densities in oblate $^{40}$Mg is small which is responsible for the almost vanishing neutron pairing gap. We see a significant neutron pairing density

Table 1: Some bulk properties of prolate and oblate $^{40}$Mg obtained by HFB-AX within the box-size of 27.6 fm. $\beta_2$ is the quadruple deformation parameter, $E_{tot}$ is the total energy, $\lambda$ is the Fermi energy, and $\Delta$ is the pairing gap. Subscripts $n$ and $p$ denote neutron and proton, respectively. All energies are in MeV.

| shape | $\beta_2$ | $E_{tot}$ | $\lambda_n$ | $\Delta_n$ | $\Delta_p$ |
|---|---|---|---|---|---|
| prolate | 0.39 | −264.14 | −0.33 | 1.23 | 0 |
| oblate | −0.32 | −262.27 | −0.79 | 0 | 0.98 |

halo as compared to the neutron normal density. In addition, we do not see an evident core-halo shape decoupling.

In Fig. 2, the transition strengths of $K = 0$ and $|K| = 1$ (the sum of $K = 1$ and $K = -1$) are shown. To see the role of accurate treatment of continuum and surface extensions, the transition strengths of prolate $^{40}$Mg are calculated with box size of 12, 21 and 27.6 fm. We see that, within a small box, the continuum discretization is not sufficient, which result in some false peaks. For instance, a false peak at 13 MeV is still present even with the box size of 21 fm. Moreover, the low-lying resonances are fragmented and less coherent without accurate continuum.

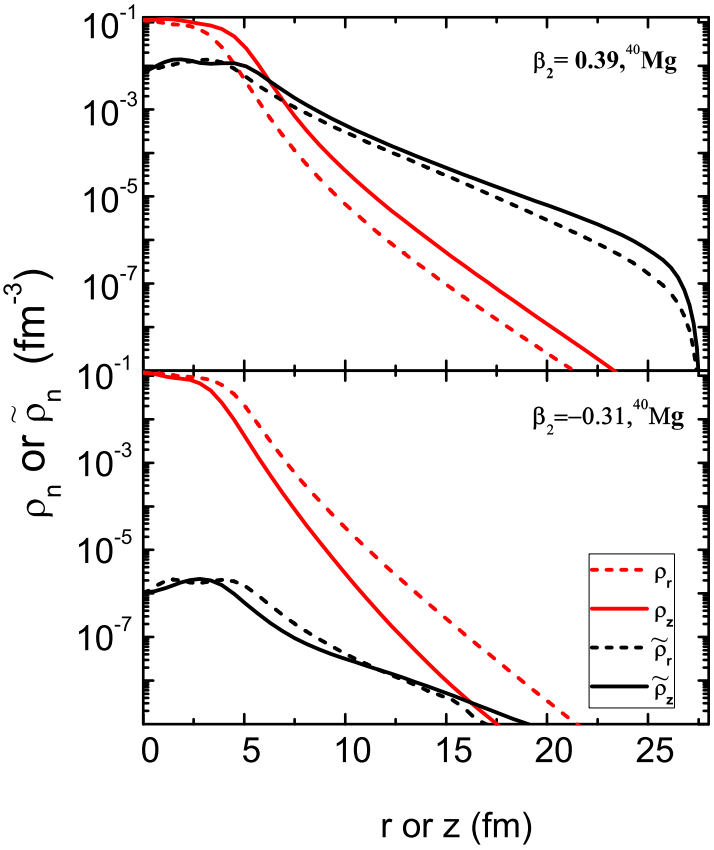


Figure 1: Neutron density $\rho_n$ and neutron pairing density $\tilde{\rho}_n$ distributions in $^{40}$Mg in prolate (upper panel) and oblate (lower panel) shapes displayed along the cylindrical coordinates $z$ (solid curve) and $r$ (dashed curve).

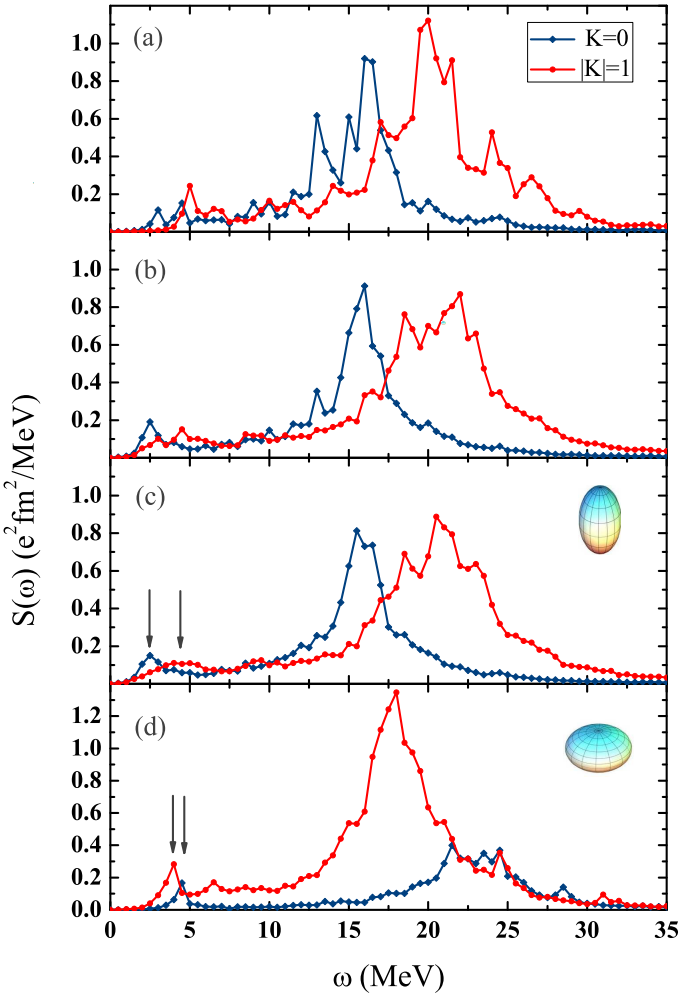


Figure 2: Calculated transition strengths of isovector dipole resonances in shape-coexisting $^{40}$Mg as functions of excitation energy. Results for (a) prolate shape with box size of 12 fm; (b) prolate shape with box size of 21 fm; (c) prolate shape with box size of 27.6 fm; (d) oblate shape with box size of 27.6 fm.

In calculations with a large coordinate space of 27.6 fm, the obtained transition strengths clearly demonstrate pygmy resonances and deformation splitting, as shown in Fig. 2 (c,d). It is known from the hydrodynamic liquid-drop model [15] that the anisotropic splitting of the dipole transition strength is approximately proportional to centroid excitation energy and deformation. It is reasonable that both cases have similar giant resonance splitting ($\delta_E \sim 5$ MeV) considering different centroid energies and deformations. Then the estimated pygmy splitting should be around 0.95 MeV for the prolate shape and 1.05 MeV for the oblate case since $^{40}$Mg actually has no evident core-halo shape decoupling [16]. However, we see the pygmy splitting of the prolate shape ($\delta_E \sim 1.4$ MeV) is significantly larger than expected while the oblate case ($\delta_E \sim 0.45$ MeV) is smaller. Obviously the hydrodynamic anisotropic splitting is not valid anymore for pygmy resonances. According to our tests, the pygmy splittings are not sensitive to pairing strengths. We speculate that the pygmy splitting is related not only with static shapes and but also with significant dynamical deformation surface effects. It will be very helpful to study the pigmy dipole resonance deformation splitting in deformed neutron-rich nuclei in high-resolution experiments.

Besides, the $|K| = 1$ dominates in the oblate case where the deformation splitting in the total cross section is not distinguishable in contrast to the prolate case.

## References


[1] P. W. Anderson, Science **177**, 393 (1972).

[2] P. Ring and P. Schuck, *The nuclear many-body problem.* Springer-Verlag, Berlin, Heidelberg, 1980.

[3] P. Avogadro and T. Nakatsukasa, Phys. Rev. C **84**, 014314 (2011).

[4] M. Stoitsov, M. Kortelainen, T. Nakatsukasa, C. Losa and W. Nazarewicz, Phys. Rev. C **84**, 041305(R) (2011); T. Nikšić, N. Kralj, T. Tutiš, D. Vretenar and P. Ring, *ibid.* **88**, 044327( 2013); H. Liang, T. Nakatsukasa, Z. Niu and J. Meng, *ibid.* **87**, 054310 (2013).

[5] J. C. Pei, M. Kortelainen, Y. N. Zhang and F. R. Xu, Phys. Rev. C **90**, 051304(R) (2014).

[6] M. Kortelainen, N. Hinohara and W. Nazarewicz, Phys. Rev. C **92**, 051302(R) (2015).

[7] K. Wang, M. Kortelainen and J. C. Pei, arXiv:1612.06019 [nucl-th] (2016).

[8] T. Baumann *et al.*, Nature **449**, 1022 (2007).

[9] J. Terasaki, H. Flocard, P-H. Heenen and P. Bonche, Nucl. Phys. A **621**, 706 (1997).

[10] R. Rodríguez-Guzmán, J. L. Eggido and L. M. Robledo, Phys. Rev. C **65**, 024304 (2002).

[11] J. C. Pei, M. V. Stoitsov, G. I. Fann, W. Nazarewicz, N. Schunck and F. R. Xu, Phys. Rev. **C78**, 064306 (2008).

[12] X. Y. Xiong, J. C. Pei and W. J. Chen, Phys. Rev. C **93**, 024311 (2016).

[13] A. Pastore, F. Barranco, R. A. Broglia and E. Vigezzi, Phys. Rev. C **78**, 024315 (2008).

[14] S. A. Changizi and C. Qi, Phys. Rev. C **91**, 024305 (2015).

[15] G. F. Bertsch and R. A. Broglia, *Oscillations in finite quantum systems.* Cambridge University Press, 1994.

[16] J. C. Pei, Y. N. Zhang and F. R. Xu, Phys. Rev. C **87**, 051302(R) (2013); Y. N. Zhang, J. C. Pei and F. R. Xu, *ibid.* **88**, 054305 (2013).